

ANOMALOUS EXTINCTION TOWARDS NGC 1938^{*}

GUIDO DE MARCHI,¹ NINO PANAGIA,^{2,3} ANTONINO P. MILONE^{4,5}

(Received 2 June 2020; Accepted 20 July 2020)
Draft version July 23, 2020

ABSTRACT

Intrigued by the extended red-giant clump (RC) stretching across the colour–magnitude diagram of the stars in a $50 \times 50 \text{ pc}^2$ region of the Large Magellanic Cloud (LMC) containing the clusters NGC 1938 and NGC 1939, we have studied the stellar populations to learn about the properties of the interstellar medium (ISM) in this area. The extended RC is caused by a large and uneven amount of extinction across the field. Its slope reveals anomalous extinction properties, with $A_V/E(B-V) \simeq 4.3$, indicating the presence of an additional grey component in the optical contributing about 30% of the total extinction in the field and requiring big grains to be about twice as abundant as in the diffuse ISM. This appears to be consistent with the amount of big grains injected into the surrounding ISM by the about 70 SNI_{II} explosions estimated to have occurred during the lifetime of the $\sim 120 \text{ Myr}$ old NGC 1938. Although this cluster appears today relatively small and would be hard to detect beyond the distance of M 31, with an estimated initial mass of $\sim 4800 M_\odot$ NGC 1938 appears to have seriously altered the extinction properties in a wide area. This has important implications for the interpretation of luminosities and masses of star-forming galaxies, both nearby and in the early universe.

Subject headings: dust, extinction — stars: formation — galaxies: stellar content - galaxies: Magellanic Clouds - galaxies: star clusters — open clusters and associations: individual (NGC1938) — globular clusters: individual: (NGC1939)

1. INTRODUCTION

NGC 1938 and NGC 1939 are two clusters in the Large Magellanic Cloud (LMC), about $36''$ apart and with a projected separation of 9 pc at the distance of the LMC ($51.4 \pm 1.2 \text{ kpc}$; Panagia et al. 1991, and updates in Panagia 1998, 1999). They are projected against the central portion of the galaxy, about $10'$ south of the LMC bar, in a region of high stellar density. We owe the first photometric study of their stellar populations to Mackey & Gilmore (2004), who observed the clusters with the *Hubble Space Telescope* (HST). These authors showed that NGC 1939 is an old globular cluster (GC) with age and metallicity comparable to those of the metal-poor Galactic GCs, confirming the earlier analysis of integrated spectroscopic data of this cluster by Dutra et al. (1999; see also Piatti et al. 2018). As for NGC 1938, from a coarse colour–magnitude diagram (CMD) Mackey & Gilmore (2004) estimated an approximate upper limit of 400 Myr to its age. The pronounced age difference between the two clusters suggests that they are not physically related and simply appear close due to a fortuitous projection effect.

A remarkable feature in the CMD of this field (see Figure 2 in Mackey & Gilmore 2004) is the prominent extension of the red-giant clump (RC), which clearly indicates that in this field there is a considerable amount of patchy extinction. De

Marchi et al. (2014, 2016) and De Marchi & Panagia (2014, 2019) have shown how in an extragalactic environment with a planar geometry such as the LMC, where all stars are practically at the same distance from us (to within a few percent, see e.g. van der Marel & Cioni 2001), the extended RC feature can be used to measure the direction of the reddening vector in the CMD, the absolute value of the extinction towards each RC star, the extinction law when multi-colour photometry is available, as well as information on the distribution and abundance of grains in the interstellar medium (ISM).

In this work, we investigate the origin of the patchy extinction causing differential reddening across the field around NGC 1938 and NGC 1939 and show that the extinction properties and the grain size distribution that they imply appear to be consistent with the number and mass of big grains that explosions of supernovae of type II (SNI_{II}) in the NGC 1938 cluster have injected into the ISM over the past $\sim 120 \text{ Myr}$.

The structure of the paper is as follows. In Section 2 we present the observations and their analysis. In Section 3 we discuss the different populations present in the field, while Section 4 is devoted to the extinction properties, which we compare with those of other regions in the LMC. A discussion and the conclusions follow, respectively, in Sections 5 and 6.

2. OBSERVATIONS AND DATA ANALYSIS

The clusters NGC 1938 and NGC 1939 were observed on 2003 July 27 with the Wide Field Channel (WFC) instrument of the Advanced Camera for Surveys on board the HST (proposal 9891). Two exposures were collected, one of 330 s through the F555W filter and one of 200 s through the F814W filter. These filters are rather similar to the standard Johnson *V* and *I* bands, although they are not identical. We retrieved the fully calibrated, flat-fielded science-ready data corrected for the effects of poor charge transfer efficiency from the Mikulski Archive for Space Telescopes. A colour-composite image obtained by combining the two exposures is shown in Figure 1. We note in passing that this field contains also parts of

¹ European Space Research and Technology Centre, Keplerlaan 1, 2200 AG Noordwijk, Netherlands; gdemarchi@esa.int

² Space Telescope Science Institute, 3700 San Martin Drive, Baltimore MD 21218, USA; panagia@stsci.edu

³ Supernova Limited, OYV #131, Northsound Rd., Virgin Gorda VG1150, Virgin Islands, UK

⁴ Dipartimento di Fisica e Astronomia, Univ. di Padova, Vicolo dell'Osservatorio 3, Padova I-35122, Italy; antonino.milone@unipd.it

⁵ Istituto Nazionale di Astrofisica – Osservatorio Astronomico di Padova, Vicolo dell'Osservatorio 5, Padova I-35122, Italy

^{*} Based on observations with the NASA/ESA *Hubble Space Telescope*, obtained at the Space Telescope Science Institute, which is operated by AURA, Inc., under NASA contract NAS5-26555

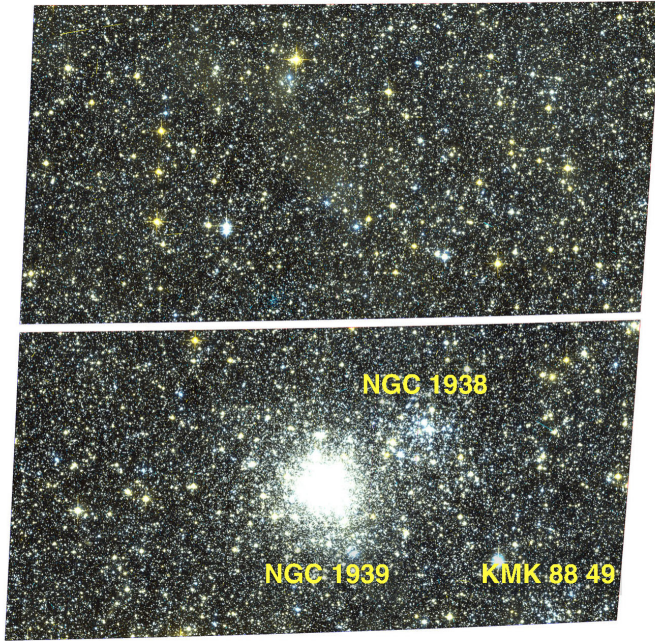


FIG. 1.— Colour composite image of the region obtained by combining the exposures in the F555W and F814W bands. The field spans approximately $205''$ or ~ 50 pc on a side. North is inclined 44° to the right of the vertical, with East to the left of North.

a third and rather small cluster, namely KMK88 49 (Kontizas et al. 1988; Piatti 2017), located near the lower right corner in Figure 1.

The astrometric and photometric analysis was carried out following the effective point spread function (ePSF) fitting procedure developed by Anderson et al. (2008) and stellar positions were corrected for geometric distortion by using the solution by Anderson & King (2006). With the exposure times used for these observations, the detector’s response for stars brighter than $m_{555} \simeq 18.1$ and $m_{814} \simeq 17.4$ becomes progressively non linear and saturates. These stars’ brightness was however completely recovered by summing over pixels into which bleeding occurred as a result of the over-saturation (see Gilliland 2004 and Anderson et al. 2008 for details). Magnitudes were calibrated in the VEGAMAG reference system following Anderson et al. (2008) and using the most recent zero-point values available through the ACS Zeropoints Calculator (see Ryon 2019). Photometric uncertainties are very small, ranging from 0.01 mag at $m_{555} = 18.2$ to 0.1 mag at $m_{555} \simeq 25$ (details are provided in Table 1). The magnitudes of stars within about 2 mag of the saturation limit are recovered with an accuracy of typically 0.02–0.03 mag.

We included in our analysis only stars that are well fitted by the ePSF routine (Anderson et al. 2008) and have small root-mean-square scatter in position measurements. This sample of stars with “high quality” photometry was selected as in Milone et al. (2009, see their Figure 1) on the basis of the various diagnostics of the astrometric and photometric quality provided by the computer programmes by Anderson et al. (2008).

3. COLOUR–MAGNITUDE DIAGRAMS OF DIFFERENT POPULATIONS

We show in Figure 2a the CMD obtained from all the stars with high-quality photometry in this field. The CMD reveals a complex population, made up of stars in different evolution-

TABLE 1
PHOTOMETRIC UNCERTAINTIES.

m_{555} (1)	σ_{555} (2)	$\sigma_{555-814}$ (3)
18.20	0.010	0.014
18.70	0.011	0.015
19.20	0.011	0.015
19.70	0.012	0.017
20.20	0.013	0.018
20.70	0.013	0.019
21.20	0.015	0.022
21.70	0.017	0.026
22.20	0.020	0.034
22.70	0.027	0.045
23.20	0.041	0.068
23.70	0.054	0.090
24.20	0.078	0.126
24.70	0.098	0.142
25.20	0.130	0.176

NOTE. — Table columns are as follows: (1) m_{555} magnitude; (2) uncertainty on the m_{555} magnitude; (3) uncertainty on the $m_{555} - m_{814}$ colour.

ary phases: a prominent and broad main sequence (MS), a double red giant branch (RGB), and a remarkably elongated RC, extending by over one magnitude in m_{555} . The broadened MS and extended RC suggest differential reddening caused by patchy absorption across the field, as Mackey & Gilmore (2004) already pointed out.

The majority of the stars in this area are LMC field objects, with a smaller contribution coming from the NGC 1938 and NGC 1939 cluster themselves. To better characterise the individual components of the overall stellar population in this area, we display in the other panels of Figure 2 the CMDs of different portions of this region.

In Figure 2b, small grey dots correspond to stars with high-quality photometry within a radius of $22''$ or 5.5 pc around the nominal centre of NGC 1939. To limit the weight of field stars and secure a higher density of cluster members, we show as thicker black dots the objects within $10''$ or 2.5 pc of the cluster centre. The resultant CMD reveals a well defined MS turn-off, at $m_{555} \simeq 22.5$, a narrow and sharp RGB, extending to $m_{555} \simeq 16$, as well as a prominent blue horizontal branch (HB), reaching down to $m_{555} \simeq 21$. As Mackey & Gilmore (2004) pointed out, the CMD of NGC 1939 resembles very closely those of metal-poor Galactic GCs such as for instance M 15 or M 92. Most of the objects located between the MS turn-off and the blue HB, which could in principle be blue stragglers (e.g. Sandage 1953; Ferraro et al. 2003), are in fact statistically compatible with being all field stars (there are 91 objects inside the wedge in Figure 2b and about 110 objects in an equally sized region located elsewhere at the NE edge of the field).

From a detailed study of the HB at RGB, Mackey & Gilmore (2004) derived for NGC 1939 a distance modulus $(m-M)_0 = 18.48 \pm 0.16$ and a colour excess $E(V-I) = 0.16$, corresponding in turn to $E(B-V) = 0.11$ and $A_V = 0.34$ adopting the Galactic extinction law for the diffuse ISM (e.g. Savage & Mathis 1979). Although this is slightly higher than the canonical $E(B-V) = 0.07$ value usually adopted for the Galactic foreground contribution to the extinction towards the LMC (e.g. Fitzpatrick & Savage 1984), the colour excess derived by Mackey & Gilmore (2004) is still within the range of literature values (see, e.g. McNamara & Feltz 1980). It is interesting to note, however, that none of the observed sequences in the CMD of NGC 1939 appear to be broadened by the differential

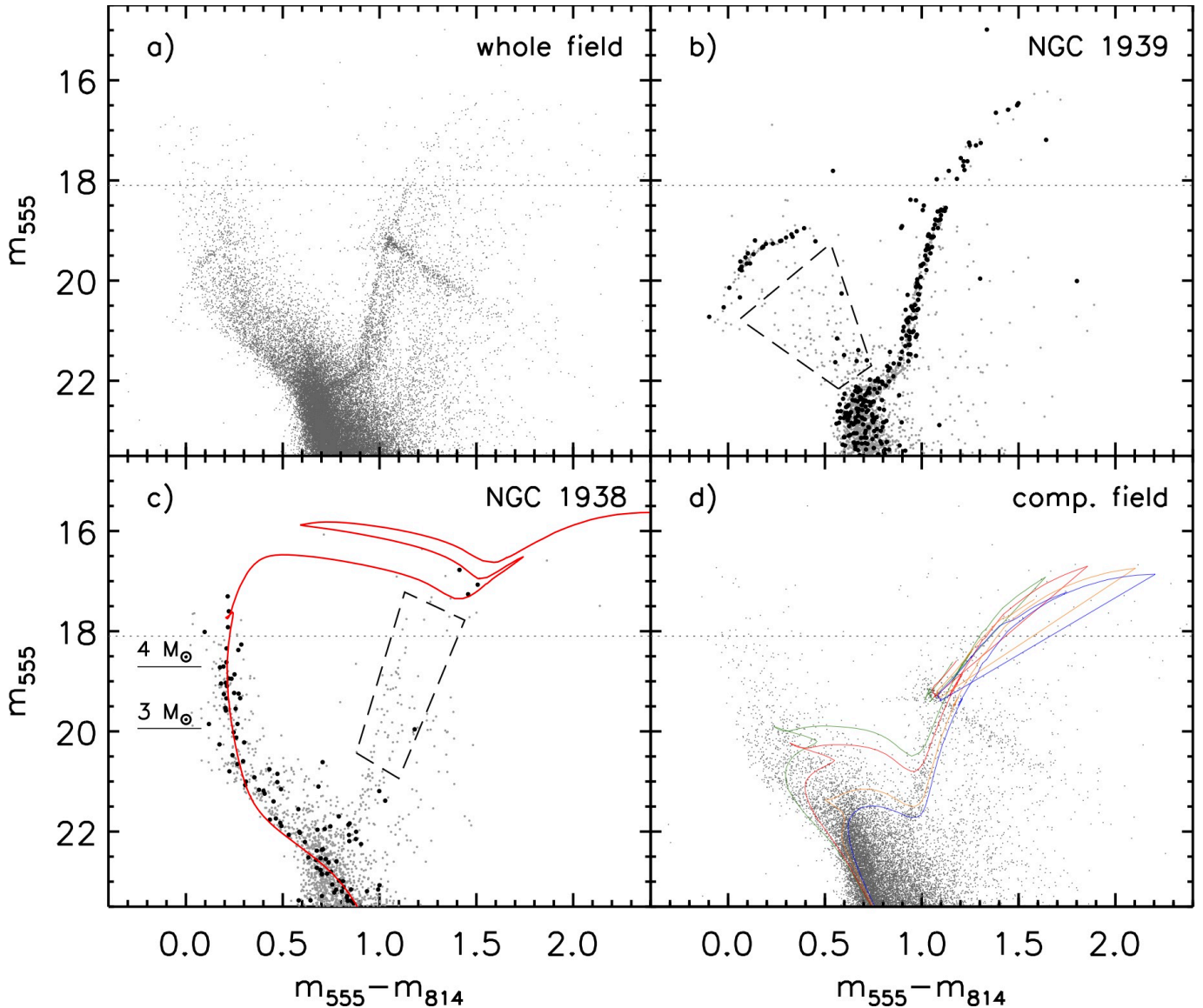


FIG. 2.— CMDs of high-quality stars in different parts of the field. In Panel a) all high-quality stars are included. In Panel b), small grey dots are used for stars within a radius of 5.5 pc of the centre of NGC 1939, while thick black dots mark objects within 2.5 pc of it. In Panel c), small grey dots indicate stars within 5.5 pc of the centre of NGC 1938 and thick black dots those within a 1.6 pc radius. The solid line shows a 120 Myr isochrone from the models of Marigo et al. (2008) for the appropriate metallicity and distance, and combined colour excess (foreground + intrinsic) of $E(V-I) = 0.39$. The CMD in Panel d) is obtained from all stars contained in the top half of Figure 1. Theoretical isochrones from the models of Marigo et al. (2008) for metallicity $Z = 0.004$ and ages of 1.5, 2, 3, and 4 Gyr are shown, respectively, in green, red, orange, and blue. In all panels the thin horizontal lines indicate the saturation level discussed in Section 2.

reddening present in the field. This promptly suggests that the NGC 1939 cluster is in the foreground of the LMC and that something else along the line of sight beyond the cluster itself is causing patchy extinction and differential reddening. Indeed, that NGC 1939 could be an outer disc cluster projected onto the LMC bar had already been suggested by Piatti et al. (2019). These authors derived a height of 450 pc out of the LMC plane based on the combined analysis of their radial velocity measurements with proper motion observations from *Gaia*.

As concerns extinction towards NGC 1938, the situation is rather different. In Figure 2c we show the CMD of all the stars with high-quality photometry in this cluster. Small grey dots mark stars within 5.5 pc of the nominal cluster centre, while the thick black dots are the more centrally located objects within a radius of $6''.5$ or 1.6 pc. The main feature in this CMD is a prominent upper MS reaching $m_{555} \simeq 17$, witness-

ing a relatively young stellar population. This is confirmed by a sparsely populated RGB in the central regions of the cluster, which is consistent with field contamination (there are 56 objects inside the dashed wedge in Figure 2c and about 44 objects in an equally sized sky area located elsewhere at the same distance from the NGC 1939 cluster).

The upper MS of NGC 1938 appears broad, witnessing the effects of patchy extinction. Furthermore, also the mean extinction towards NGC 1938 appears considerably higher than the $E(V-I) = 0.16$ value measured by Mackey & Gilmore for NGC 1939. We can satisfactorily reproduce the NGC 1938 young MS and what appear to be red supergiants with a theoretical isochrone from Marigo et al. (2008) for an age of 120 Myr, metallicity $Z = 0.007$, and adopting for the LMC a distance modulus $(m-M)_0 = 18.55$ (Panagia 1998). However, to obtain a good fit an extra $E(V-I) = 0.23$ component of colour excess is needed in addition to the fore-

ground $E(V-I) = 0.16$ mentioned above. If the more canonical $E(V-I) = 0.11$ is used for the foreground extinction to the LMC, the contribution of the extra component grows to $E(V-I) = 0.28$ with no noticeable difference in the quality of the isochrone fit.

As we will show in Section 4, also the value of R_V in NGC 1938 is larger than the canonical $R_V = 3.1$ characteristic of the diffuse ISM. We note that isochrones for younger or older ages would give a progressively less good fit. The only existing estimate of the age of NGC 1938 is that of Mackey & Gilmore (2004), who set an upper limit of 400 Myr to it. Our isochrone best fit, however, indicates a definitely younger age for this cluster, of the order of 120 Myr. The isochrone suggests that the heaviest stars still on the MS have a mass of approximately $4.5 M_\odot$. The emerging picture is one in which NGC 1938 is considerably younger and more extinguished than NGC 1939 and likely closer to the LMC than the latter, most likely inside the LMC disc itself.

To compare this situation with that of the surrounding field, in Figure 2d we show the CMD obtained from all the stars with high-quality photometry falling in the ACS detector not including the two clusters (top half of Figure 1). The CMD shows the structures typical of the LMC field population, including a MS, RGB, and RC, which in this field all appear to be severely affected by differential reddening. To guide the eye, we show theoretical isochrones for ages of 1.5, 2, 3, and 4 Gyr from the same models of Marigo et al. (2008), shown respectively in green, red, orange, and blue. Measurements reported in the literature concur in assigning ages of 1–3 Gyr to the intermediate-age populations in the field of the LMC (e.g., Westerlund et al. 1995; Elson et al. 1997; Geha et al. 1998), and evidence points to a major star formation event occurred some 2 Gyr ago. As for the metallicity, we adopt as representative for this older stellar population $Z = 0.004$, which is the preferred value for field stars in 30 Dor (De Marchi et al. 2014) and is typical for the LMC (e.g., Hill et al. 1995; Geha et al. 1998).

Adopting for the foreground component of the extinction the $E(V-I) = 0.16$ value derived by Mackey & Gilmore (2004) for NGC 1939, the isochrones provide a good fit to the RGB and to the location of the ‘head’ of the RC at $m_{555} - m_{814} \simeq 1.1$ and $m_{555} \simeq 19.3$. Nevertheless, the over-density of points in the CMD departing from the head of the RC and extending by more than one magnitude in m_{555} is a clear and unmistakable sign of patchy extinction. In the next section we will address the use of this feature to derive the direction of the reddening vector from the data themselves.

We note that the CMD of KMK8849, not shown in Figure 2, is marginally different from that of field stars in the same area. From the analysis of its integrated colours, Piatti (2017) estimated an age of $\gtrsim 500$ Myr, while the total mass is estimated by Popescu et al. (2012) to be around $800 M_\odot$, also from integrated colours.

4. RED CLUMP STARS AS EXTINCTION PROBES

The RC is populated by stars that are experiencing their central He-burning phase (e.g. Cannon 1970). The remarkably consistent location of these stars in the CMD makes the RC feature a powerful tool to probe distance and reddening. A detailed study of the behaviour of the mean RC as a function of age, metallicity, and star-formation history is provided by Girardi & Salaris (2001) and Salaris & Girardi (2002). Populations containing RC stars with different age and metallicity will produce a slightly elongated shape for the RC, but, as

shown by De Marchi et al. (2014), in the LMC these effects account for at most 0.2 mag in the F555W and F814W bands when both the metallicity and age vary by a factor of two.

Also differences in distance between RC members in the same field could cause the RC to extend in the CMD, as is commonly observed for field RC stars in the Milky Way. But in order to cause a one magnitude extension, such as the one observed in Figure 2, the RC objects at the most distant end must be $\sqrt{2.5}$ times farther away than those at the near end. In the case of the LMC, this would require the galaxy to extend about 30 kpc along the line of sight and is at odds with the accepted almost planar geometry. Van der Marel & Cioni (2001) derived an inclination angle of $\sim 35^\circ$ for the plane of the LMC and a disc scale height of $\lesssim 0.5$ kpc. A somewhat larger estimate of the scale height comes from the recent work of Jacyszyn–Dobrzeńska et al. (2016), who probed the three-dimensional structure using classical Cepheids. Their data show that, when considering the entire extent of the LMC, the standard deviation on Cepheids distances is about 2 kpc, due to the inclination of the galaxy with respect to the plane of the sky, but it becomes obviously smaller when individual lines of sight are considered. For instance, within a radius of 50 pc ($200''$) of the centre of our region, the catalogue of Jacyszyn–Dobrzeńska et al. (2016) contains six classical Cepheids, with a median distance of 51.4 kpc and a standard deviation of 0.75 kpc, implying a scale height of the order of ~ 1 kpc. Even in this case, without differential reddening the expected elongation of the RC would still be less than 0.1 mag. So the morphology of the RC observed in Figure 2d is not consistent with any physically reasonable extension of the LMC along the line of sight and can only be the result of high and patchy extinction.

In these circumstances, the RC shape in the CMD can be used to measure the direction of the reddening vector in a fully empirical way (Nataf et al. 2013; De Marchi et al. 2014). An efficient and accurate method to achieve this is the application of the unsharp-masking technique. Extensive details on the method are provided by De Marchi et al. (2016). In summary, unsharp-masking makes an image of the CMD sharper by overlapping to the image itself a mask consisting of an inverted blurred version of the image. To this aim, each object in the CMD is mapped to a two-dimensional array (the CMD image) with a sampling of 0.01 mag in colour and magnitude and the array is then convolved with a narrow Gaussian beam. The convolution assigns to each point in the CMD the proper resolution, including uncertainties on the photometry, and here we used $\sigma = 0.08$ mag, or about three times the typical photometric uncertainty. To create the mask, we convolved the array also with a wider Gaussian beam, with $\sigma = 0.3$ mag, and subtracted the mask from the CMD image. These operations are analytically equivalent to convolving the CMD with a kernel represented by the difference between two Gaussian beams with different σ (see De Marchi et al. 2016 for further details).

The result of unsharp-masking the CMD of field stars is displayed in Figure 3. The substructures and local density enhancements appear better defined. Although all features were already present in Figure 2d, the high density of more uniformly distributed objects in their surroundings made them more difficult to distinguish and characterise quantitatively. It is now possible to solidly determine the ridge line of the extended RC and derive from it the direction of the reddening vector, without even having to know the location of the

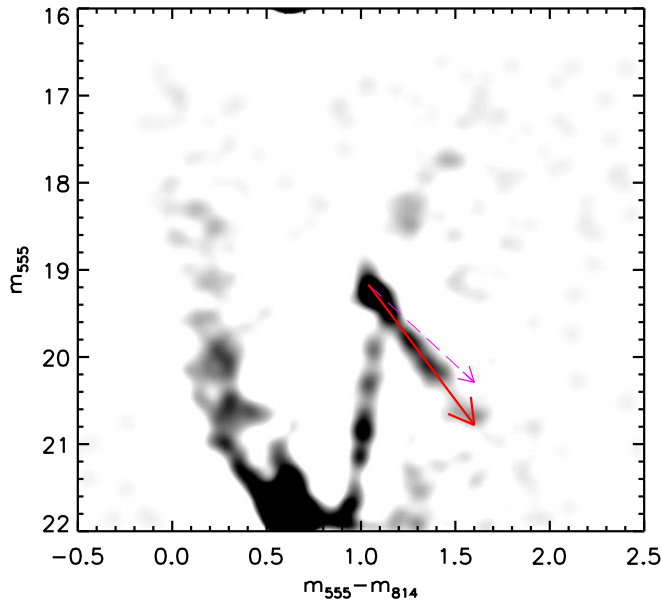


FIG. 3.— Same CMD as in Figure 2d after unsharp masking. The thick arrow marks the ridge along the elongated RC, while the thin dashed arrow shows the direction of the reddening vector in the diffuse ISM, corresponding to $R_V = 3.1$.

nominal unextinguished RC, since the head of the distribution empirically defines its position. The best linear fit along the extended RC (thick arrow in Figure 3) provides the slope of the reddening vector and is obtained by applying weights proportional to the local object density. It is ~ 1.5 times steeper than the reddening vector for the diffuse ISM in these bands (thin dashed arrow). The slope along the extended RC corresponds to the ratio of absolute (A) and selective (E) extinction in the specific bands and its value is

$$\frac{A_{555}}{E(m_{555} - m_{814})} = 2.99 \pm 0.12. \quad (1)$$

The corresponding slope in the $m_{814}, m_{555} - m_{814}$ plane is 1.94 ± 0.08 .

These slopes are in excellent agreement with those measured in the same bands in the central regions of the 30 Dor nebula (see De Marchi & Panagia 2014), respectively 2.97 ± 0.08 and 1.96 ± 0.06 . The more numerous set of filters available for those observations of 30 Dor allowed De Marchi & Panagia (2014) to measure the extinction curve over the wavelength range $0.3 - 1.6 \mu\text{m}$ and to determine the extinction values at the wavelength corresponding also to the traditional Johnson B band. When the extinction properties are expressed in the form of the ratio

$$R_\lambda \equiv \frac{A_\lambda}{E(B-V)}, \quad (2)$$

where A_λ is the extinction in the specific band and $E(B-V)$ the colour excess in the Johnson B and V bands, the resulting value for 30 Dor is $R_V = 4.5 \pm 0.2$.

We note in passing that Merica-Jones et al. (2017) suggested that the steeper slope of the extended RC in the CMD of 30 Dor measured by De Marchi & Panagia (2014), and the correspondingly large R_V value, might in fact result from the line-of-sight depth of the LMC, which could in principle introduce an apparent grey contribution to the extinction curve. Their models suggest that a depth of 5 ± 1 kpc (full width at half maximum) is required to account for the observed RC

shape in 30 Dor, assuming an otherwise standard extinction law (i.e. $R_V = 3.1$). However, there are several problems with this interpretation. First, the measurements of the scale height of the LMC along individual lines of sight do not support such a large depth (see above). Second, the morphology of the extended RC predicted by the models of Merica-Jones et al. (2017; see their Figure 7) bears no resemblance to what is actually observed in the CMD of this field nor in that of the 30 Dor region (see also De Marchi et al. 2016). In particular, our observations do not show the populous group of RC stars predicted by those model to appear about 0.5 mag brighter than the nominal location of the RC and caused by unextinguished RC stars closer to the observer. In all our observations, the observed “head” of the RC is exactly where theory of stellar evolution predicts it to be for stars about 1–3 Gyr old at the nominal distance of the LMC (e.g. Girardi & Salari 2001; Salari & Girardi 2002). Furthermore, if the effects of differential reddening were compounded with those of considerable line-of-sight depth, the RC would not develop along a straight line and would appear curved in the CMD. The fact that the observations show a tight linear distribution instead indicates that the effects of distance, if present, are marginal.

Finally, and perhaps most importantly, the extinction law derived by De Marchi & Panagia (2014) from the morphology of the extended RC in 30 Dor agrees very well with the one measured in the same field by Maíz-Apellániz et al. (2014) with a completely independent method. These authors obtained the extinction law from the observations of 83 stars of spectral type O and B in the inner $2'$ radius of 30 Dor, using spectroscopy and near infrared (NIR) photometry from the VLT-FLAMES Tarantula Survey (Evans et al. 2011) as well as HST photometry at optical wavelengths (De Marchi et al. 2011). Following a Bayesian approach to derive the so-called extinction without standards (Fitzpatrick & Massa 2005), the shape of the extinction curve that they obtain is in excellent agreement with that of De Marchi & Panagia (2014; see their Figure 4) at optical wavelengths and shows a similar decay in the NIR, where De Marchi & Panagia (2014) measured the extinction curve directly from the HST observations while Maíz-Apellániz et al. (2014) assumed it to be that of Cardelli et al. (1989). The 50 stars with the smallest uncertainties on extinction in the sample of Maíz-Apellániz et al. (2014) indicate $R_V = 4.4 \pm 0.2$, fully matching the $R_V = 4.5 \pm 0.2$ found by De Marchi & Panagia (2014). None of these curves is compatible with the standard extinction law (i.e. $R_V = 3.1$) suggested by Merica-Jones et al. (2017).

As discussed by De Marchi & Panagia (2014; see also De Marchi et al. 2014, 2016), the extinction curve of 30 Dor is fully compatible with the contribution of two components: one being the extinction of the standard diffuse ISM (e.g., Cardelli et al. 1989), and the other an additional grey component accounting for about 1/3 of the total extinction. The similarity between the slopes of the reddening vectors measured in the F555W and F814W bands in the NGC 1938/1939 field and in 30 Dor suggests that also in this region the extinction is affected by an additional grey component at optical wavelengths. Actually, with the extinction law of 30 Dor (De Marchi & Panagia 2014), a value of $R_V = 4.3 \pm 0.3$ would result in a ratio $A_{555}/E(m_{555} - m_{814}) = 2.99 \pm 0.12$, as measured in the NGC 1938/1939 field. The grey component would account for about 30% of the total extinction and the diffuse ISM for the remaining $\sim 70\%$ (since $R_V = 3.1$ in the diffuse ISM). This implies an overabundance of big grains with respect to the Galactic and LMC ISM. In the next section we

will discuss the origin and implications of an elevated value of R_V in this region.

5. DISCUSSION

A large value of R_V has long been known to characterise the ISM in star-forming regions in the Milky Way (MW; e.g., Baade & Minkowski 1937; Watson & Costero 2011 and references therein), so it does not surprise that a large R_V value is also found in 30 Dor, where massive star formation is currently ongoing (e.g. Walborn 1991). What could appear unexpected, however, is to find an equally large value of R_V in the field containing NGC 1938 and NGC 1939, where the most recent star-formation episode dates back to some 120 Myr ago (see Figure 2c). However, as we will show, this value of R_V appears to be quantitatively consistent with the recent star formation history of NGC 1938.

Measuring $R_V = 4.3$ in this field suggests that, like in the case of 30 Dor, also here the extinction law is flatter than in the diffuse Galactic ISM, where $R_V = 3.1$ (e.g. Cardelli et al 1989). Such a flatter, greyer extinction requires big grains to dominate the distribution function of grain sizes (e.g. van de Hulst 1957). In the case of 30 Dor, from the study of the extinction curve at optical and near infrared wavelength De Marchi & Panagia (2014) concluded that the relative abundance of big grains must be a factor of 2.2 higher than in the diffuse ISM. In principle, big grains could be produced through mechanisms such as coalescence of small grains, small grain growth, and selective destruction of small grains. However, from a study of the ultraviolet extinction properties of three massive stars in 30 Dor, De Marchi & Panagia (2019) showed that the excess of big grains does not come at the expense of small grains, which are still at least as abundant in 30 Dor as in the diffuse ISM of the LMC. They concluded instead that the dominant mechanism is fresh injection of big grains with radius $a \gtrsim 0.05 \mu\text{m}$, and that explosions of massive stars as SNe II are a natural process to account for it, since massive star formation is still ongoing in 30 Dor (e.g. Walborn 1991; De Marchi et al. 1993).

Indeed, observations with ALMA and/or *Herschel* revealed up to $\sim 0.5 M_\odot$ of dust and possibly more formed in situ in core-collapse SNe ejecta, such as SN 1987A (Matsuura et al. 2011; Gomez et al. 2012; Indebetouw et al. 2014), the Crab Nebula, and Cassiopeia A (Barlow et al. 2010; Gomez et al. 2012; De Looze et al. 2017). Although the exact size distribution of dust formed in supernova remnants is uncertain (e.g., Temim & Dwek 2013; Owen & Barlow 2015; Wesson et al. 2015; Bevan & Barlow 2016), grains larger than $\sim 0.05 \mu\text{m}$ appear to be both produced during and preserved after the explosion of SNe II (e.g. Gall et al. 2014; Silvia et al. 2010; Biscaro & Cherchneff 2016). Therefore, even though coalescence and growth of small grains remain possible, SNe II explosions appear a likely and rather natural source of big grains in regions that in the recent past underwent massive star formation.

For 30 Dor, De Marchi & Panagia (2014, 2019) discovered that at wavelengths longer than the V band the effects of big grains in the extinction curve start to saturate and that beyond $\sim 1 \mu\text{m}$ the extinction curve tapers off as $\lambda^{-1.7}$, following almost exactly the properties of the extinction law in the diffuse ISM (e.g. Cardelli, Clayton & Mathis 1989). These findings provide direct information on the physical characteristics of the additional component of big grains, including their size ($a \gtrsim 0.05 \mu\text{m}$) and relative abundance with respect to the diffuse ISM (a factor of about 2 larger). The stark similarities

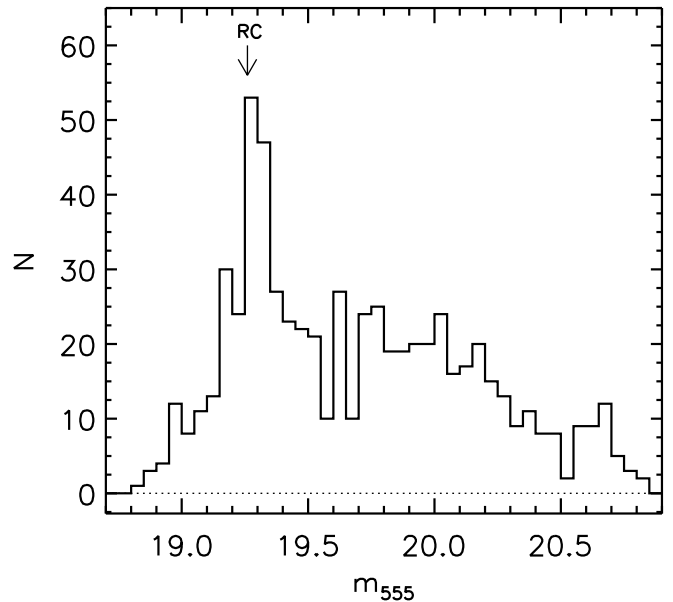


FIG. 4.— Histogram of the m_{555} magnitudes of stars within a ± 0.4 mag band around the reddening vector shown in Figure 3. The peak at $m_{555} \simeq 19.3$ agrees very well with the expected magnitude of the ‘nominal’ RC in this field (black arrow).

between the reddening vectors measured in the F555W and F814W bands in 30 Dor and in NGC 1938, as well as the similar chemical composition, strongly suggest that the extinction law in this cluster will remain comparable also at other wavelengths. Therefore, as mentioned above, it is reasonable to assume that a similar size and abundance of the big grains also apply to the field of NGC 1938.

In order to put this hypothesis on firmer observational grounds, we explore whether the excess of big grains implied by $R_V = 4.3$ as measured in this field is consistent with that expected from SNe II explosions in NGC 1938. We start by calculating the mass of grains along the line of sight.

In general, at short enough wavelengths the extinction cross section σ_{ext} of a grain tends asymptotically to twice its geometric cross section $\sigma_{\text{geom}} = \pi a^2$, where a is the grain’s radius (see, e.g., van de Hulst 1957; Greenberg 1968; Draine & Lee 1984). At longer wavelengths, where scattering becomes less important and the extinction is dominated by pure absorption, the cross section is smaller than σ_{geom} and approaches $\sigma_{\text{geom}} \times 2\pi a/\lambda$. Conveniently enough, the transition between the two regimes occurs approximately at $\lambda_0 \sim 2\pi a$. So in the ideal case of a fixed grain size, around wavelength λ_0 one would expect a change of slope in the extinction curve, with a steepening at longer wavelengths. Therefore, adopting once again as representative of this field the extinction law of 30 Dor (De Marchi & Panagia 2019), the saturation effect seen at wavelengths longer than the V band suggests that $\lambda_0 \simeq 0.55 \mu\text{m}$ and thus the presence of grains of radius $a \simeq 0.09 \mu\text{m}$ or $9 \times 10^{-6} \text{cm}$. Their cross section σ_{ext} is thus $2\pi a^2 = 5.1 \times 10^{-10} \text{cm}^2$.

The number of such grains along the line of sight can be derived as the ratio of the optical depth τ_V of the big grains component and σ_{ext} . As for τ_V , it can be obtained directly from the measured A_V value pertaining just to the additional component of big grains. The amount of A_V in this field varies considerably, as indicated by the extent of the RC. In Figure 4 we display a histogram of the m_{555} magnitudes of stars within a ± 0.4 mag band around the reddening vector shown in Fig-

ure 3. The peak in the distribution observed at $m_{555} \simeq 19.3$ is in excellent agreement with the magnitude of the ‘nominal’ RC derived by De Marchi & Panagia (2014) for field stars in the 30 Dor region, taking into account the somewhat larger foreground extinction in this field ($A_V = 0.34$; Mackey & Gilmore 2004) compared with the $A_V = 0.22$ value applicable to the 30 Dor area, as discussed in Section 3. Many RC stars are displaced by reddening to fainter magnitudes by up to about 1.5 mag. The median extinction value of RC stars is $A_V = 0.36$ (see Figure 4), which we will use as characteristic value for this field. We note that the distribution of extinction values for RC stars around the ~ 500 Myr old KMK88 49 is in full agreement with that of the rest of the field. But inside the NGC 1938 cluster the median extinction value is higher and $A_V = 0.65$ is the amount indicated by the best fit to the cluster MS (see Figure 2c), once the $A_V = 0.34$ contribution of the Galactic foreground extinction is removed. It is not surprising that the extinction is higher in NGC 1938 since, as we will show, it appears that the cluster itself is the source of the elevated and anomalous extinction in this field.

With a characteristic $A_V = 0.36$ value in this field, the fraction contributed by big grains amounts to $A_V = 0.10$, as we showed in Section 4 that the extra component of big grains account for about 30% of the total extinction. In turn, the optical depth of big grains is $\tau_V = 1.086 \times A_V = 0.11$ and the number of big grains along the typical line of sight in this region is then $n = \tau_V / \sigma_{\text{ext}} = 2.1 \times 10^8$. Considering that the area A covered by the observations is $50 \times 50 \text{ pc}^2$ or $2.4 \times 10^{40} \text{ cm}^2$, the total number N of big grains in the region is $N = n \times A = 5.1 \times 10^{48}$. With a typical density of $\sim 2.7 \text{ g cm}^{-3}$ (Panagia 1974; Draine & Lee 1984), the mass of a typical grain is $m = 8.2 \times 10^{-15} \text{ g}$. Hence the total mass of the extra component of big grains is $M = N \times m = 4.2 \times 10^{34} \text{ g}$, or about $21 M_\odot$.

If each SNe II explosion accounts for about $0.3 M_\odot$ of dust in big grains (see above), about 70 such explosions would be needed over the lifetime of NGC 1938. Although the calculations are necessarily approximate, this number is indeed fully compatible with the number of SNe progenitors implied by the mass function of the cluster.

Using the 120 Myr isochrone in Figure 2d as a reference, within a radius of $22''$ or 5.5 pc of the centre of NGC 1938 there are 86 stars with masses in the range $3 - 4 M_\odot$. To remove field-star contamination, we calculated the number of objects in the same region of the CMD for an area of the same size located near the NE edge of the image, finding on average 9 stars. This brings to 77 the effective number of NGC 1938 stars with masses in the range $3 - 4 M_\odot$. These objects are all still on the MS (see Figure 2c) and are bright enough to not suffer the effects of photometric incompleteness. With 77 stars in this mass range, adopting a standard IMF (Kroupa 2001) with power-law index $\gamma = -2.3$ for stars above $0.5 M_\odot$ results in about ~ 66 SNe II progenitors, i.e. stars initially more massive than $\sim 8 M_\odot$. Considering the unavoidable approximations involved in this computation, the result appears in surprisingly good agreement with the number of SNe II explosions needed to account for the observed additional component of big grains in the ISM of this region. Therefore, SNe II are a plausible source of the additional big grains.

The fact that the extinction is patchy means that the total amount of dust along different lines of sight is not the same, but the tight linear RC feature in the CMD suggests that the grains are well mixed, with more or less similar distributions

of grain sizes along neighbouring lines of sight in this field. Hence the value of R_V appears to be uniform across the area. This is probably not unexpected if SNe II are at the source of the elevated value of R_V : at the age of NGC 1938 there should have been sufficient time for grains to mix and be processed in the ISM since the first SNe II explosions some 100 Myr ago, at least over the field covered by our observations.

6. CONCLUSIONS

In summary, the flatter extinction curve implied by the $R_V = 4.3$ value measured in this field suggests that big grains are about twice as abundant than in the diffuse ISM and this appears to be consistent with the grain contributed by SNe II explosions throughout the life of NGC 1938. The initial total mass of the cluster, assuming a power-law IMF index $\gamma = -1.3$ in the stellar mass range $0.08 - 0.5 M_\odot$ (Kroupa 2001), is about $4800 M_\odot$. This places the cluster in the intermediate mass range: about an order of magnitude smaller than massive Galactic star-forming clusters such as Westerlund 1 ($\sim 50000 M_\odot$; Andersen et al. 2017), Westerlund 2 ($\sim 36000 M_\odot$; Zeidler et al. 2017), and NGC 3603 ($\sim 15000 M_\odot$; Harayama et al. 2008), NGC 1938 is still a factor of a few more massive than the Orion Nebula Cluster (ONC, $\sim 1000 M_\odot$; Da Rio et al. 2012).

An anomalous extinction curve (with $R_V \gtrsim 5$) has long been known to characterise the ONC (e.g. Baade & Minkowski 1937; Sharpless 1952; Johnson & Mendoza 1964; Breger et al. 1981), and has been attributed to grain growth in the dense prestellar molecular cloud through accretion from the gas phase or grain coagulation (e.g. Cardelli & Clayton 1988). Other examples of star-forming regions in dense molecular clouds with anomalous extinction are Taurus (Whittet et al. 2000) and Cep OB3b (Allen et al. 2014). While NGC 1938 is about 5 times more massive than the ONC, it has likely formed in an equally dense molecular cloud. What is surprising, however, is that the excess of big pre-stellar grains persists some ~ 120 Myr after the cluster’s formation: by now the molecular cloud has long completely dissipated, thereby removing the conditions for grains to grow. If instead the origin of the overabundance of big grains in NGC 1938 is the fresh injection of big grains by SNe II explosions, as we suggest, it appears easier to understand an anomalous extinction curve well past the end of the star formation process: SNe II explosions happen after the formation of the cluster and continue to replenish the ISM with fresh new grains for up to ~ 40 Myr, when all SNe II progenitors have exploded (e.g. Marigo et al. 2017). Once injected, the additional big grains will continue to pollute the ISM for a non-negligible amount of time. A study of a complete sample of SN remnants in the Magellanic clouds by Temim et al. (2015) estimates grain lifetimes in the range $\sim 20 - 70$ Myr, with $\sim 50\%$ uncertainties. Big grains from SN II explosions are thus not unexpected even in the ~ 120 Myr old NGC 1938.

Therefore, an anomalous extinction could be a common and long-lasting characteristic of star forming regions that are sufficiently massive to host SNe II. An intermediate-mass cluster such as NGC 1938 appears to be able to considerably alter the conditions of the surrounding ISM. Indeed, in a forthcoming paper (De Marchi et al., in prep.) we will show that the LMC regions with a prominent extended RC and apparently anomalous extinction (including also relatively young clusters such as NGC 1756, NGC 1858, NGC 1872, and NGC 1903) are all characterised by extended dust emission detected in the far infrared, which is not present in regions of low total extinction.

Of course, the anomalous extinction caused by the pollution by large grains will affect the observations of all regions in the background. This has important consequences for our ability to derive meaningful values of the mass or the star formation rates from the study of extragalactic stellar populations, regardless of their age. Normally extinction correction is needed in order to derive the intrinsic luminosity of the stars. To this aim, the extinction properties in the region must be known, including the value of R_V . This requires a careful analysis of the stellar populations, including those in surrounding regions, to identify signs of intermediate-mass clusters formed in the past few 100 Myr that could act as potential ISM polluters. This is not always possible. For instance, with a current total mass of about $3300 M_\odot$, a cluster like NGC 1938 is easy to identify in the Magellanic clouds, but already at the distance of M 31 it would be problematic to recognise clusters with the mass of the ONC at ages $\lesssim 200$ Myr (Johnson et al. 2015), due to detection and resolution limits. At larger distances it becomes increasingly difficult to identify

even more massive or younger clusters, and a larger uncertainty on the population's physical parameters as derived from photometry and line luminosities cannot be avoided. Paradoxically, the situation might become less uncertain in the early universe if the Magellanic Clouds are indeed representative of these low-metallicity primeval environments (e.g. Simon et al. 2007). In that case, since young unresolved massive star-forming regions are the only objects detectable at high redshift, our work suggests that a value of R_V not smaller than ≈ 4.5 appears most likely.

We are grateful to an anonymous referee whose comments have helped us improve the presentation of this work. APM acknowledges support from the European Research Council (ERC) under the European Union's Horizon 2020 research innovation programme (Grant Agreement ERC-StG 2016, No 716082 'GALFOR', <http://progetti.dfa.unipd.it/GALFOR>), by the MIUR through the FARE project R164RM93XW 'SEMPLICE' and the PRIN programme 2017Z2HSMF.

REFERENCES

- Allen, T., Prchlik, J., Megeath, S., et al. 2014, *ApJ*, 786, 113
 Andersen, M., Gennaro, M., Brandner, W., et al. 2017, *A&A*, 602, A22
 Anderson, J., King, I. 2006, Instrument Science Report ACS 2006-01, (Baltimore: STScI)
 Anderson, J., Sarajedini, A., Bedin, et al. 2008, *AJ*, 135, 2055
 Baade, W., Minkowski, R. 1937, *ApJ*, 86, 123
 Barlow, M., Krause, O., Swinyard, B., et al. 2010, *A&A*, 518, L138
 Bevan, A., Barlow, M. 2016, *MNRAS*, 456, 1269
 Biscaro, C., Cherchneff, I. 2016, *A&A*, 589, A132
 Breger, M., Gehrz, R., Hackwell, J. 1981, *ApJ*, 248, 963
 Cannon, R. 1970, *MNRAS*, 150, 111
 Cardelli, J., Clayton, G. 1988, *AJ*, 95, 516
 Cardelli, J., Clayton, G., Mathis, J. 1989, *ApJ*, 345, 245
 Da Rio, N., Robberto, M., Hillenbrand, L., Henning, T., Stassun, K. 2012, *ApJ*, 748, 14
 De Looze, I., Barlow, M., Swinyard, B., et al. 2017, *MNRAS*, 465, 3309
 De Marchi, G., Nota, A., Leitherer, C., Ragazzoni, R., Barbieri, C. 1993, *ApJ*, 419, 658
 De Marchi, G., Panagia, N. 2014, *MNRAS*, 445, 93
 De Marchi, G., Panagia, N. 2019, *ApJ*, 878, 31
 De Marchi, G., Panagia, N., Girardi, L. 2014, *MNRAS*, 438, 513
 De Marchi, G., Panagia, N., Sabbi, E., et al. 2016, *MNRAS*, 455, 4373
 De Marchi, G., Paresce, F., Panagia, N., et al. 2011, *ApJ*, 739, 27
 Draine, B., Lee, H. 1984, *ApJ*, 285, 89
 Dutra, C., Bica, E., Clariá, J., Piatti, A. 1999, *MNRAS*, 305, 373
 Elson, R., Gilmore, G., Santiago, B. 1997, *MNRAS*, 289, 157
 Evans, C., Taylor, W., Hénault-Brunet, V., et al. 2011, *A&A*, 530, A108
 Ferraro, F., Sills, A., Rood, R., Paltrinieri, B., Buonanno, R. 2003, *ApJ*, 588, 464
 Fitzpatrick, E., Massa, D. 2005, *AJ*, 130, 1127
 Fitzpatrick, E., Savage, B. 1984, *ApJ*, 279, 578
 Gall, C., Hjorth, J., Watson, D., et al. 2014, *Nature*, 511, 326
 Gilliland, R. 2004, Instrument Science Report ACS 2004-01, (Baltimore: STScI)
 Geha, M., Holtzman, J., Mould, J., et al. 1998, *AJ*, 115, 1045
 Girardi L., Salaris M., 2001, *MNRAS*, 323, 109
 Gomez, H., Krause, O., Barlow, M., et al. 2012, *ApJ*, 760, 96
 Greenberg, J. M. 1968, in *Nebular and interstellar matter*, Ed. B. Middlehurst, L. Aller (Chicago: Univ. Chicago Press), 221
 Harayama, Y., Eisenhauer, F., Martins, F., 2008, *ApJ*, 675, 1319
 Hill, V., Andrievsky, S., Spite, M. 1995, *A&A*, 293, 347
 Indebetouw, R., Matsuura, M., Dwek, E., et al. 2014, *ApJ*, 782, L2
 Jacyszyn-Dobrzniecka, A., Skowron, D., Mróz, P., et al. 2016, *Acta Astr.*, 66, 149
 Johnson, H., Mendoza v., E. 1964, *BOTT*, 3, 331
 Johnson, L., Seth, A., Dalcanton, J., et al. 2015, *ApJ*, 802, 127
 Kroupa, P. 2001, *MNRAS*, 322, 231
 Mackey, A., Gilmore, G. 2004, *MNRAS*, 352m 153
 Maíz Apellániz, J., Evans, C., Barbá, R., et al. 2014, *A&A*, 564, A63
 Marigo P., Girardi L., Bressan A., et al. 2008, *A&A*, 482, 883
 Marigo, P., Girardi, L., Bressan, A., et al. 2017, *ApJ*, 835, 77
 Matsuura, M., Dwek, E., Meixner, M., et al. 2011, *Sci*, 333, 1258
 McNamara, D., Feltz, K. 1980, *PASP*, 92, 587
 Merica-Jones, P., Sandstrom, K., Johnson, L., et al. 2017, *ApJ*, 847, 102
 Nataf, D. M., Gould, A., Fouqué, P., et al. 2013, *ApJ*, 769, 88
 Owen, P., Barlow, M. 2015, *ApJ*, 801, 141
 Panagia, N. 1973, *AJ*, 78, 929
 Panagia, N. 1974, *ApJ*, 192, 221
 Panagia N. 1998, *Mem. Soc. Astron. Ital.*, 69, 225
 Panagia N. 1999, in Chu Y.-H., Suntzeff N., Hesser J., Bohlender D., eds, *Proc. IAU Symp. 190, New Views of the Magellanic Clouds* (San Francisco: Astron. Soc. Pac.), 549
 Panagia N., Gilmozzi R., Macchetto F., Adorf H.-M., Kirshner R., 1991, *ApJ*, 380, L23
 Piatti, A. 2017, *A&A*, 606, A21
 Piatti, A., Alfaro, E., Cantat-Gaudin, T. 2019, *MNRAS*, 484, L19
 Piatti, A., Hwang, N., Cole, A., Angelo, M., Emptage, B. 2018, *MNRAS*, 481, 49
 Popescu, B., Hanson, M., Elmegreen, G. 2012, *ApJ*, 751, 122
 Ryon, J. 2019, *ACS Instrument Handbook*, Version 19 (Baltimore: STScI), <https://hst-docs.stsci.edu/acsihb>
 Salaris M., Girardi L., 2002, *MNRAS*, 337, 332
 Sandage, A. 1953, *AJ*, 58, 61
 Savage, B., Mathis, J. 1979, *ARA&A*, 17, 73
 Sharpless, S. 1952, *AJ*, 116, 251
 Silvia, D., Smith, B., Shull, J. 2010, *ApJ*, 715, 1575
 Simon, J., Bolatto, A., Whitney, B., et al. 2007, *ApJ*, 669, 327
 Temim, T., Dwek, E. 2013, *ApJ*, 774, 8
 Temim, T., Dwek, E., Tchernyshyov, K., et al. 2015, *ApJ*, 799, 158
 van de Hulst, H. 1957, *Light Scattering by Small Particles* (New York: John Wiley & Sons)
 Van der Marel, R., Cioni, M. 2001, *AJ*, 122, 1807
 Walborn, N. 1991, in *IAU Symp. 148, The Magellanic Clouds*, ed. R. Haynes & D. Milne (Dordrecht: Kluwer), 145
 Watson, A., Costero, R. 2011, *RMxAC*, 39, 9
 Wesson, R., Barlow, M., Matsuura, M., Ercolano, B. 2015, *MNRAS*, 446, 2089
 Westerlund, B., Linde, P., Lynga, G. 1995, *A&A*, 298, 39
 Whittet, D., Gerakines, P., Hough, J., Shenoy, S. 2000, *ApJ*, 547, 872
 Zeidler, P., Nota, A., Grebel, E., et al. 2017, *AJ*, 153, 122